# Magneto-optic Kerr effect in a spin-polarized zero-moment ferrimagnet

Karsten Fleischer,[1,2] Naganivetha Thiyagarajah,[3] Yong-Chang Lau,[3] Davide Betto,[3] Kiril Borisov,[3] Christopher C. Smith,[1] Igor V. Shvets,[1] J.M.D. Coey,[3] and Karsten Rode[3]

[1] *School of Physics, Trinity College Dublin*
[2] *Dublin City University*
[3] *CRANN and School of Physics, Trinity College Dublin*

(Dated: October 10, 2018)

The magneto-optical Kerr effect (MOKE) is often assumed to be proportional to the magnetisation of a magnetically ordered metallic sample; in metallic ferrimagnets with chemically distinct sublattices, such as rare-earth transition-metal alloys, it depends on the difference between the sublattice contributions. Here we show that in a highly spin polarized, fully compensated ferrimagnet, where the sublattices are chemically similar, a signal is observed even when the net moment is negligible. We analyse the spectral ellipsometry and MOKE of $Mn_2Ru_xGa$, and show that this behaviour is due to a highly spin-polarized conduction band dominated by one of the two manganese sublattices ($4c$) which creates helicity-dependent reflectivity dominated by a broad Drude tail. Our findings open new prospects for studying spin dynamics in the infra-red.

## I. INTRODUCTION

Spin valves, where angular momentum can be transferred from a reference layer to a free layer, are expected to form the basis of future memory devices and oscillators operating in the far infra-red frequency domain.[1] The key materials properties necessary to achieve these frequencies are a high Fermi-level spin polarization $P$; low net magnetization $M_s$ and a high effective magnetic anisotropy field $\mu_0 H_\mathrm{k}$. A compensated ferrimagnetic half metal where negligible magnetization can be obtained, coupled with full ($P = 100\,\%$) spin polarization, would be an ideal choice.[2]

Such a material was suggested by van Leuken and de Groot[3] in 1995, but the first experimental evidence was only provided by the work of Kurt *et al.*[4] in 2014. We have recently shown that the material, $Mn_2Ru_xGa$ (MRG), shows negligible $M_s$ over a wide temperature and thermal treatment range;[5,6] high spin polarization[4] as reflected in the anomalous Hall effect;[7] produces sizeable magnetoresistive effects in spin electronic structures[8] such as magnetic tunnel junctions;[9] and proposed an *ab initio* model reconciling the experimental observations with density functional theory (DFT) band structure calculations.[10]

Time-resolved magneto-optical Kerr/Faraday effect is particularly suited to determine the Larmor frequency of thin-film samples, especially when the resonance frequency exceeds the experimental range of cavity- or network-analyser-based techniques. The unique properties of MRG indicate that the material may be a candidate for low-power all-optical switching as the magnetic compensation temperature $T_\mathrm{comp}$ can be tuned to lie just above room temperature,[11] but these measurements on new materials are complicated by the lack of an accepted, wavelength-dependent optical model.

Ferrimagnets with two chemically distinct sublattices, notably the rare-earth transition metal alloys have been investigated by spectroscopic MOKE.[12,13] The spectral response of the $4f$ and $3d$ elements allow the temperature dependence of the Kerr effect of each sublattice to be determined. The new aspect we present here is that in a ferrimagnet with chemically identical, but structurally inequivalent, sublattices it is possible to track the spin polarization associated with only one of the sublattices.

We first show that even at magnetic compensation, MRG exhibits a clear Kerr rotation ($\theta_K$). Spectroscopic ellipsometry, in combination with the spectroscopic polar MOKE[14] allow us to determine the diagonal ($\tilde{\varepsilon}_{xx}$) and off-diagonal ($\tilde{\varepsilon}_{xy}$) dielectric tensor components as a function of Ru concentration $x$. Polar MOKE is often used simply to measure hysteresis loops using monochromatic light, and the spectroscopic variant provides more specific information on the sites responsible for the magnetic response. Our measurements show a clear correlation between the infrared Kerr rotation and the electrically-measured Hall angle, providing contactless, optical measurements of this quantity. The experimentally determined, optical model developed here will facilitate measurements in the time- and frequency-domains, that can advance the development of spin electronic devices operating in the far infra-red frequency range.

## II. SAMPLE DETAILS

The thin-film samples studied here were grown on MgO (001) substrates by dc magnetron sputtering at 250 °C substrate temperature in a 'Shamrock' system with a base pressure of $2 \times 10^{-8}$ Torr. The films were co-sputtered from Ru and $Mn_2Ga$ targets. The Ru concentration was controlled by varying the $Mn_2Ga$ target plasma power while keeping that of the Ru fixed. The samples were then capped with a protective 2 nm layer of amorphous aluminium oxide. The crystal structure, lattice parameters and strain of the films were characterised by $2\theta - \theta$ X-ray diffraction and reciprocal space mapping using a Bruker D8 Discover instrument, with a

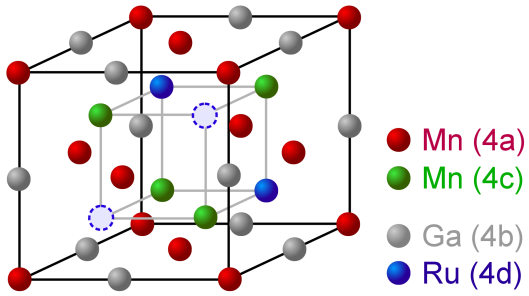


FIG. 1. Schematic of the MRG crystal structure. There are three filled fcc sublattices (red: Mn-site (4*a*), grey: Ga-site (4*b*), green: Mn-site (4*c*)). Ruthenium occupies the remaining fcc sublattice (blue: Ru-site (4*d*)). The two Mn sites are non equivalent in the structure as the 4*a*-site has only Ga as nearest neighbour, while the 4*c*-site Ru, or vacancies (dashed circles) depending on the Ru content $x$.

monochromatic copper $K_{\alpha 1}$ source. We found that the in-plane lattice constant $a$ is $0.5956\,\text{nm} = \sqrt{2}a_{\text{MgO}}$ for all samples, indicating that MRG grows epitaxially on MgO with its basal plane rotated by 45° with respect to the substrate. The out-of-plane parameter $c$ varies between 0.598 nm and 0.618 nm, depending on Ru concentration and film thickness ($\sim$ 26 to 81 nm). The measurement confirms a slight, substrate-induced, tetragonal distortion of the cubic structure. An illustration of the crystal is given in FIG. 1.

In order to determine the Ru concentration, we deposited four MRG samples with varying $Mn_2Ga$ target power and a pure Ru film. The density and thickness were then measured using X-ray reflectivity (XRR). Based on the measured density and lattice parameters of these five control samples, we established a relation between X-ray density and Ru concentration $x$, against which all the samples were calibrated. The transport properties of the thin films were measured on non-patterned films in a Quantum Design physical properties measurement system (PPMS) at temperatures ranging from 10 to 400 K in an applied magnetic field, $\mu_0 H$, of up to 12 T.

## III. EXPERIMENTAL DETAILS

Both ellipsometry and magneto-optical Kerr spectroscopy were used to determine the optical and magneto-optical properties of the films. Spectroscopic MOKE was recorded at near-normal incidence with a in-house built reflectance anisotropy spectrometer, based on the design of Aspnes.[15] Light from a Xe lamp passes through a Rochon $Mg_2F$ polariser and is reflected from the sample. The beam then passes through a photo-elastic modulator (PEM), an analysing polariser and a monochromator before finally reaching a diode detector system. All measurements were performed from 0.35 to 5 eV, using a Bentham TMc300 triple-grating monochromator and three individual photo-diodes (InAs, InGaAs, Si). The procedure for extracting the MOKE rotation has been discussed elsewhere.[16–18] All samples where measured at room temperature in remanence (no external field). Samples were magnetised before these measurements in fields of up to 12 T at room temperature. Selected sample have also been magnetised at 200 K.

To correct for any set-up or non-magnetic anisotropy, we recorded spectra for two orthogonal in-plane directions as well as for samples magnetized in opposite directions. The spectra obtained by reversal of $\vec{M}$, were strictly equal to those derived from a rotation of the sample of 90° around the optical axis.

Due to larger errors in the Kerr-ellipticity measurement in a PEM setup without *in-situ* magnetisation reversal, only the Kerr rotation ($\theta_K$) will be discussed.

A Sopra GESP 5 spectroscopic ellipsometer was used over an energy range from 1.5 to 5 eV with incidence angles of 70°, 75° and 80°. Both, the thin film dielectric function ($\tilde{\varepsilon}_{xx}, \tilde{\varepsilon}_{xy}$), as was derived from the raw measurements by minimising the deviation between measured ellipsometric data ($\tan\Psi, \cos\Delta$) over the whole spectral range, as well as all three angles. Full transfer matrix calculations of the air/$AlO_x$/MRG/MgO layer stack have to be evaluated, as in contrast to simple bulk samples no analytical expression for the relationship between measured $\tan\Psi, \cos\Delta$, and $\theta_K$ exists. The spectral shape of $\tilde{\varepsilon}$ was simulated by a standard Drude-like component plus three harmonic oscillators (Drude-Lorentz oscillator). To reduce uncertainties in $\tilde{\varepsilon}_{xx}$, only the MRG layer was modelled. The sample thickness and interface roughness, as measured by XRR was used as input parameters together with the known bulk dielectric functions of the MgO substrate and the $AlO_x$ capping layer.

In thin film structures, the $\theta_K$ spectra depend not only on the off-diagonal dielectric tensor components $\tilde{\varepsilon}_{xy} = iQm_z\tilde{\varepsilon}_{xx}$ of the magnetic material but also on the overall reflectance of the stack. Knowing the diagonal components $\tilde{\varepsilon}_{xx}$ from the ellipsometric model, the measured $\theta_K$ spectral signature can then also be modelled, and hence $\tilde{\varepsilon}_{xy}$ determined using the same methodology without skewed results caused by variations in $\tilde{\varepsilon}_{xx}$ and sample thickness/roughness and modulation of the overall reflectivity.[19–21]

For all optical models, the MRG and $AlO_x$ thicknesses determined by XRR were treated as fixed parameters. All interfaces have been treated as sharp, while the dielectric function of the $AlO_x$ coating has been modelled by a Bruggeman effective medium of crystalline $Al_2O_3$ and air with a fill factor set to the density ratio of the XRR fitted capping layer and crystalline $Al_2O_3$. We treat the MRG to be perfectly cubic, as the deviation from cubic symmetry due to epitaxial strain of $\sim 1\,\%$[22] is well below the sensitivity of our instrument.

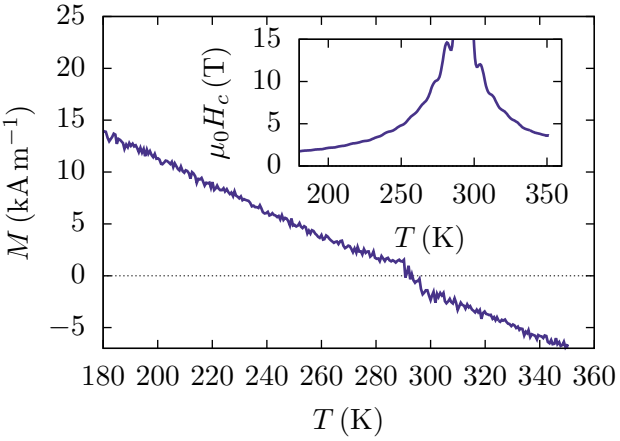


FIG. 2. SQUID magnetometry of sample with $T_{\rm comp}$ close to RT. The net magnetisation of the sample was measured at remnance on warming after saturation at low temperature. In the inset we show an estimate of the coercive field, $\mu_0 H_c$, as a function of temperature. Around room-temperature, even 15 T is insufficient to saturate the magnetisation.

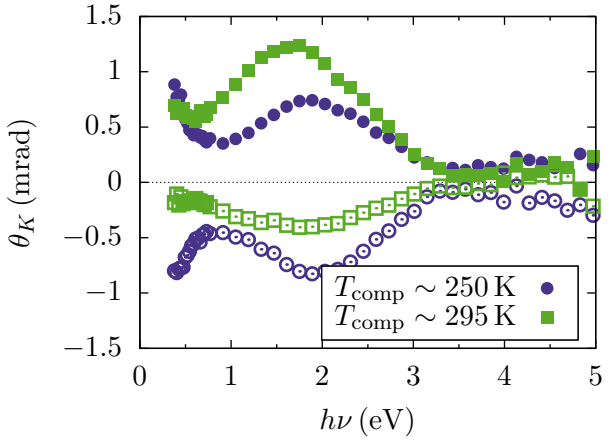


FIG. 3. Room-temperature Kerr rotation as a function of photon energy for samples with $T_{\rm comp} \sim 295$ K and 250 K, respectively. The samples were first magnetised at RT in a field of $\mu_0 H = 2$ T (above $T_{\rm comp}$, open symbols). Subsequently, the samples were remagnetised, this time well below $T_{\rm comp}$ ($T_{\rm sat} = 200$ K, filled symbols). Although all measurements are done at RT, the sign of the MOKE signal is reversed depending on whether magnetisation is carried out above or below $T_{\rm comp}$. When $T_{\rm comp} \sim 295$ K, full saturation is only achieved when magnetised well below $T_{\rm comp}$.

## IV. MOKE: DIRECT MEASUREMENTS

Due to the different crystallographic sites occupied by the two magnetic sublattices in ferrimagnets, the temperature dependence of the magnetisation of the two sublattices differ. Generally, perfect compensation and zero net moment occurs only at a specific temperature ($T_{\rm comp}$) where the magnitudes of the two magnetic sublattices are equal but opposite in sign. For MRG this temperature depends on both Ru content $x$ and the biaxial substrate-induced strain.

Upon crossing $T_{\rm comp}$ in zero applied field the net magnetisation changes sign whereas the spin-dependent DOS remains unchanged because the individual sublattices have not changed direction. We therefore expect that the sign of any property that depends on the spin-resolved DOS such as MOKE, tunnel magneto-resistance (TMR) and anomalous Hall effect, will exhibit opposite signs depending on whether the sample was magnetised below or above $T_{\rm comp}$.[7,9]

In FIG. 2 we show the temperature dependence of the net magnetic moment of an MRG sample with $T_{\rm comp} \sim 295$ K. The inset gives an estimate of the coercive field as a function of temperature. Close to $T_{\rm comp}$, the anisotropy field $\mu_0 H_k$ diverges, and as the coercive field is directly related to the anisotropy field, the sample cannot be magnetically saturated in this temperature range.

We now compare MOKE spectra of two samples with $T_{\rm comp}$ of 295 K and 250 K, respectively. The data are shown in FIG. 3. When magnetised at RT, *i.e.* above $T_{\rm comp}$, both samples exhibit clear MOKE *negative* in sign. The sample with $T_{\rm comp}$ closest to RT appears to have a reduced magnitude. We then magnetise both samples well below their respective $T_{\rm comp}$, $T_{\rm sat} = 200$ K, and subsequently warm to RT in zero applied field. This procedure ensures that while the net magnetic moment changes sign when crossing $T_{\rm comp}$, the spin-dependent density of states (DOS) remains unchanged. We then record MOKE spectra at RT. As can be seen from FIG. 3, both samples exhibit a change of sign as expected, and crucially, the sample with $T_{\rm comp} \sim 295$ K and thus near zero net moment now displays as strong or stronger MOKE signal as the sample measured further away from $T_{\rm comp}$. This set of measurements proves that MOKE in MRG depends on the spin-dependent DOS, and not the net magnetic moment; and furthermore even when the net magnetic moment is zero, the MOKE signal is clearly observed.

We note here that disproportionality between the remnant magnetization and the polar MOKE measured during a hysteresis loop have been observed previously, in different circumstances.[23,24] This was attributed to coupling, *during switching*, of the in-plane magnetization and the polar MOKE through higher order terms. It was observed in highly anisotropic exchange-biased materials and only during switching. The samples measured here do not exhibit uniaxial in-plane anisotropy, and they are all measured at remanence.

In order to pinpoint the origin of MOKE in MRG, we recorded angle and energy dependent ellipsometry, which in combination with the measured Kerr rotation allow us to determine all matrix elements of the dielectric tensor.

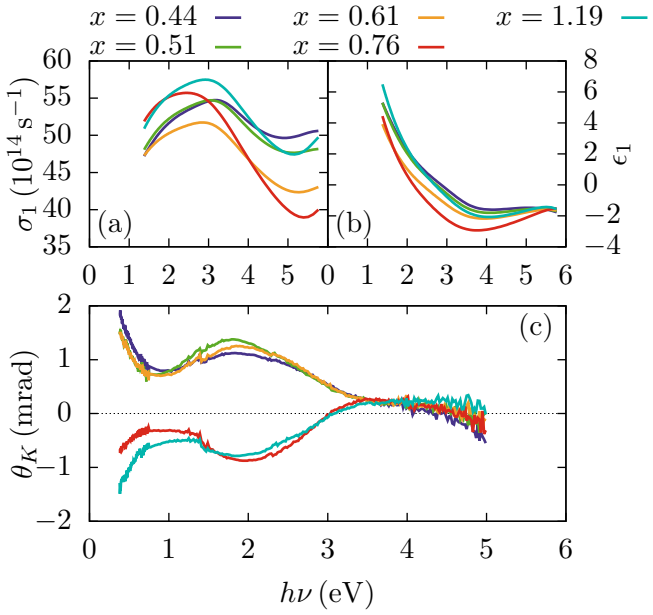


FIG. 4. (a) and (b): Imaginary and real components of the diagonal tensor elements $\tilde{\varepsilon}_{xx}$ of the dielectric function of MRG as a function of photon energy and Ru concentration $x$. The imaginary part is shown in terms of optical conductivity ($\sigma_1 = \varepsilon_2\omega/4\pi$)[25], to highlight the small differences between samples.The behaviour is dominated by the Drude-like metallic response, with smaller deviations caused by interband transitions. (c) MOKE spectra for the same series of samples used to infer the off-diagonal $\tilde{\varepsilon}_{xy}$ tensor elements.

## V. OPTICAL MODEL

We have shown that MOKE is not determined by the net magnetic moment, but depends on the spin dependent DOS in MRG. MOKE measurements alone are insufficient to determine $\tilde{\varepsilon}_{xx}$ and $\tilde{\varepsilon}_{xy}$. We therefore first use spectroscopic ellipsometry to determine $\tilde{\varepsilon}_{xx}$ and subsequently develop the optical model including the off-diagonal tensor elements $\tilde{\varepsilon}_{xy}$ for MRG.

In FIG. 4 we show the dielectric function $\tilde{\varepsilon}_{xx}$ as extracted from least square fits of the measured $\tan\Psi$ and $\cos\Delta$ for a set of samples with varying Ru concentration $x$. Our optical model, used for both $\tilde{\varepsilon}_{xx}$ and $\tilde{\varepsilon}_{xy}$ is based on the following considerations:

For metallic materials such as MRG the dielectric response is usually dominated by a strong Drude-like tail caused by free electron absorption, also known as *intraband* transitions.[26] This contribution is the reason why the imaginary part of $\tilde{\varepsilon}_{xx}$ of MRG does not tend towards zero ($\sigma \sim 45\times10^{14}\,\mathrm{s}^{-1}$ at $h\nu = 1\,\mathrm{eV}$) in the infra-red region. Furthermore, there are absorption features in the visible (VIS - peaks $\sim 2.3\,\mathrm{eV}$) which we attribute to interband transitions on both Mn sites, ultra-violet (UV $\sim 3.2\,\mathrm{eV}$) due to Ga, and a deep ultra-violet contribution (DUV $> 5.5\,\mathrm{eV}$) necessary to account for the line shape but that cannot be assigned to a specific element. The assignment of the VIS structure to Mn interband transitions is motivated by several experimental and theoretical findings, including similar spectral features in bulk $\alpha$-Mn,[25] a strong peak in the unoccupied density of states in *ab-initio* calculations for bulk Mn,[27] and finally the similarity in the shift of the energetic position of the VIS peak with increasing Ru concentration, following the same trend as that seen in site-selective XAS/XMCD measurements on $Mn_2Ru_xGa$.[5]

To minimize the number of free parameters, we therefore describe the diagonal part of the dielectric function via one Drude-like oscillator at $\omega = 0\,\mathrm{eV}$, and three broad harmonic oscillators ($\Gamma > 6\,\mathrm{eV}$) in the VIS, UV and DUV ranges, respectively.

The Kerr spectra show strong features in the IR and the VIS regions, associated with the Drude-tail and the Mn, respectively, but no separate features in the UV and DUV. As the magnetism in MRG is dominated by Mn in two antiferromagnetically coupled sub-lattices, $\tilde{\varepsilon}_{xy}$ can be described in more detail. We associate the single, broad, VIS oscillator observed in ellipsometry at $h\nu \sim 2.3\,\mathrm{eV}$ with two individual components in the Kerr spectra (NIR and VIS in FIG. 5, bottom panel), which we assign to the spin-dependent transitions on the Mn-4*c* and Mn-4*a* site. In agreement with our assignment above of the UV and DUV transitions to non-magnetic components, no separate UV and DUV oscillators are required to describe $\tilde{\varepsilon}_{xy}$.

This assignment is motivated by our earlier X-ray absorption measurements[5] where we find that the final states of the $2p \rightarrow 3d$ transitions of Mn in the two sites are only separated by approximately 1 eV, and no circular magnetic dichroism on the Ga $L_{2,3}$ edges nor on the Ru $M_{4,5}$ edges, as well as the dielectric functions of Mn[25] and Ga[28].

In FIG. 5 we show an example of a fit to the model described above. Having established the diagonal tensor elements $\tilde{\varepsilon}_{xx}$ we then model the off-diagonal terms which we plot as the expected Kerr rotation $\theta_K$ (the real part of the complex Kerr rotation). The agreement between the experimental data and the optical model is excellent, indicating that our model is well justified as well as highlighting the predominant role of Mn in MRG magnetisation. The (extrapolated) steep increase in MOKE in the IR and towards DC ($h\nu \rightarrow 0\,\mathrm{eV}$) is clearly an effect of the highly spin-polarised conduction band, as reflected by the Drude contribution to both diagonal and off-diagonal tensor elements.

Our modelling allows us to study in finer detail the behaviour of the spectral components of the ellipsometry and MOKE as a function of Ru concentration $x$ (FIG. 4).

When the Ru concentration $x$ changes from 0.44 to 1.19, the oscillator associated with Ga (UV) changes position only slightly from 3.4 to 3.2 eV whereas the oscillator associated with Mn (VIS), exhibits a stronger trend and moves from 3.0 to 2.2 eV with increasing $x$. With increasing Ru content, the electronic occupation of Mn is increasing linearly, wheres that of Ga remains constant. The (small) changes associated with Ga are thus

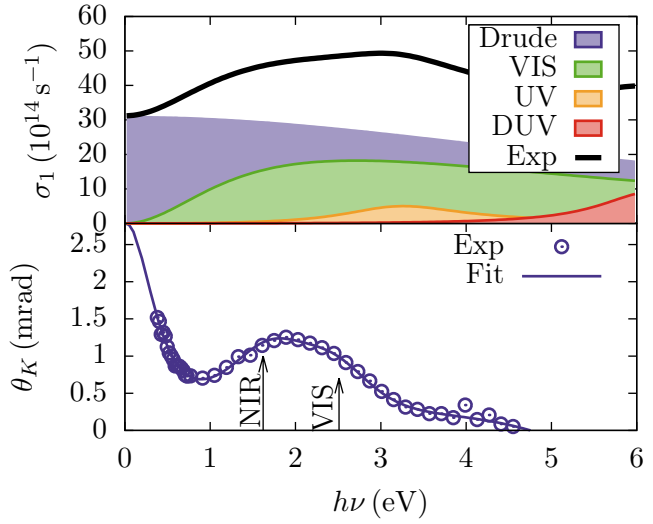


FIG. 5. Complete optical model and experimental data for an MRG sample with $x = 0.61$. (Top) Experimentally observed optical conductance (line) and the fitted contributions from the four harmonic oscillators (areas) described in the text. (Bottom) Experimental Kerr rotation (points) and fit to the data (line) based on the optical model described in the main text.

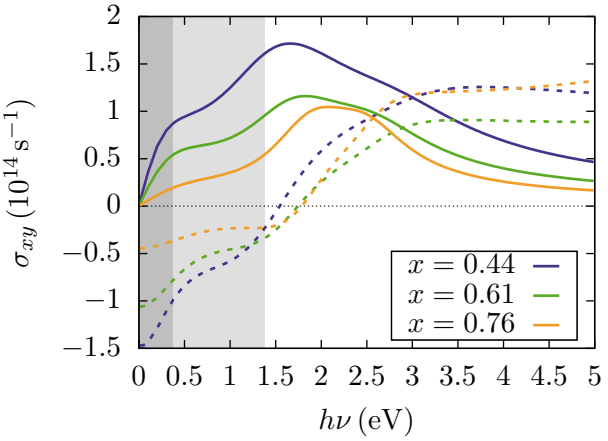


FIG. 6. $\sigma_{xy}$ extracted from the optical model for three different Ru concentrations $x$. The real and imaginary parts are plotted in solid and broken lines, respectively. In the light and dark grey areas, the curves are extrapolated from the experimentally available range in ellipsometry and MOKE, respectively. Please not that $\mathrm{Im}(\sigma_{xy})$ is only determined up to a potential integrational constant

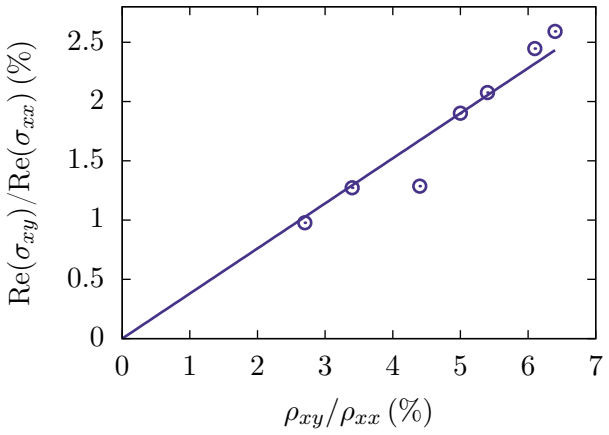


FIG. 7. Ratio of the real part of the off-diagonal and on-diagonal terms of the dielectric tensor extrapolated to 0.4 eV plotted as a function of the electrically measured anomalous Hall angle. The straight line is a fit to the data, and provides a guide to the eye. As expected, the DC limit of the magneto-optical characterisation agrees very well with the values obtained through electronic transport measurements.

due to increasing tetragonality of the crystal structure while those associated with Mn correlate directly with the band filling. As described above, the MOKE in MRG is dominated by the contributions of Mn, both through the spin polarisation of the conduction band as well as single-ion transitions. The two oscillators used to describe these transitions in MOKE can therefore be associated with Mn in the $4c$ position ($\sim 1.7$ eV - NIR) and in the $4a$ position ($\sim 2.5$ eV - VIS). Due to the half-metallic nature of the sample, when Ru content is increased, the electronic occupation of Mn in the $4c$ position increases leading to a blue shift (from 1.4 to 1.8 eV) of the oscillator associated with this position. Simultaneously, adding Ru decreases the spin-gap[10] thereby inducing a red shift (from 2.7 to 2.4 eV) of the oscillator associated with Mn in the $4a$ position. More details on the optical model parameter as function of Ru concentration $x$ are found in the supplemental information.[29]

In FIG. 6 we show the off-diagonal component of the dielectric tensor as a function of photon energy, extracted from the fit of the experimental ellipsometry and MOKE data, in terms of $\sigma_{xy}$. Unlike the raw MOKE spectra, differences between different compositions are now clearly visible, and highlight, independently of our discussion focussed on MRG, the need to employ robust optical modelling when reporting MOKE data on thin film samples of even slightly varying thickness.

We finally turn to a comparison of the DC limit of the magneto-optical properties with the anomalous Hall angle measured by standard electronic magnetotransport. As outlined above, our optical model describes the behaviour of MRG fully in the spectral region measured, and we therefore expect that extrapolation outside this region should accurately predict the behaviour at different photon energies. The lower limit is of course DC where optical measurements are not possible, but where we can record magnetotransport, in particular anomalous Hall effect.[7] The ratio $\rho_{xy}/\rho_{xx}$ is the Hall angle, the DC limit of the ratio $\mathrm{Re}(\sigma_{xy})/\mathrm{Re}(\sigma_{xx})$. In FIG. 7 we plot the ratio determined from the extrapolation of our optical model as a function of the Hall angle determined by

magnetotransport measurements as described in II. The ratio was evaluated at $h\nu = 0.4\,\mathrm{eV}$ as we only need to extrapolate $\sigma_{xx}$ and not $\sigma_{xy}$ at this energy. As expected we observe a strong correlation between the two measurements, most certainly because the two effects share a common origin; the high spin polarisation of the conduction band. The deviations from a perfectly proportional behaviour is due to small differences in the scattering matrices that have a big influence in transport measurements whereas they do not influence the values obtained by optical means. We also emphasize that whereas electronic transport probes the entire thickness of a metallic film, MOKE and ellipsometry only probe the skin-depth, which varies with photon energy, found here to be 5 nm at 2 eV and 40 nm at 0.4 eV.

## VI. CONCLUSION

We have shown that MOKE in zero-moment half metals persists, even when the net magnetic moment crosses zero, and that its origin is dominated by the highly spin-polarised conduction band associated in MRG with Mn in the 4*c* site.[5] The sign of the MOKE depends on whether the sample was magnetised above or below its compensation temperature, as the process of magnetisation sets the direction of the axis of quantization for the spin-polarised density of states.

By combining spectroscopic ellipsometry and MOKE it was possible to construct an optical model that identifies the optically active components of MRG, and we were able to use this to infer the full parameterized dielectric tensor as a function of photon energy in the range 0 to 5 eV. The model is deliberately designed to minimize the number of free parameters, yet it captures with reasonable accuracy both the nonmagnetic and the magnetic contributions for MRG in the spectral range measured. Based on the model, we compare the results obtained by optical means with the anomalous Hall angle recorded by electronic transport measurements. Although the DC limit is far beyond our experimentally available range, the extrapolated values of $\sigma_{xy}$ agree remarkably well with those obtained by transport measurements.

Differences between magnetic properties observed by anomalous Hall effect and MOKE are often used nowadays as a fingerprint of topological electronic transport.[30] An extension of this study with a more in-depth comparison between the two in high and zero applied magnetic fields, may allow an unambiguous determination of the scattering coefficients that lead to topologically driven spin structures in for example non-collinear ferrimagnets, as a complete optical model is necessary to disentangle effects that depend solely on differences in sample thickness and reflectivity from those that are purely magnetic in nature.

Finally, this work opens a path to study the behaviour of magnetic domains in antiferromagnets by MOKE microscopy,[31] while the shown spectral dependence highlights photon energies most suitable for pump-probe based time dependent measurements.[32]

## ACKNOWLEDGMENTS

This project has received funding from the European Union's Horizon 2020 research and innovation programme under grant agreement No 737038. KF and IVS acknowledges support from Science Foundation Ireland (SFI), grant number 06/IN.1/I91. DB gratefully acknowledges funding from the Irish Research Council. This work was supported by SFI through AMBER and through grant number 16/IA/4534.

[1] D. Betto, K. Rode, N. Thiyagarajah, Y.-C. Lau, K. Borisov, G. Atcheson, M. Žic, T. Archer, P. Stamenov, and J. M. D. Coey, AIP Adv. **6**, 055601 (2016), 10.1063/1.4943756.

[2] M. Hakimi, M. Venkatesan, K. Rode, K. Ackland, and J. M. D. Coey, J. Appl. Phys. **113**, 17B101 (2013), 10.1063/1.4794744.

[3] H. van Leuken and R. A. de Groot, Phys. Rev. Lett. **74**, 1171 (1995).

[4] H. Kurt, K. Rode, P. Stamenov, M. Venkatesan, Y.-C. Lau, E. Fonda, and J. M. D. Coey, Phys. Rev. Lett. **112**, 027201 (2014).

[5] D. Betto, N. Thiyagarajah, Y.-C. Lau, C. Piamonteze, M.-A. Arrio, P. Stamenov, J. Coey, and K. Rode, Phys. Rev. B **91**, 094410 (2015).

[6] K. E. Siewierska, G. Atcheson, K. Borisov, M. Venkatesan, K. Rode, and J. M. D. Coey, IEEE Transactions on Magnetics **53**, 1 (2017).

[7] N. Thiyagarajah, Y.-C. Lau, D. Betto, K. Borisov, J. Coey, P. Stamenov, and K. Rode, Appl. Phys. Lett. **106**, 122402 (2015).

[8] K. Borisov, G. Atcheson, G. D'Arcy, Y.-C. Lau, J. M. D. Coey, and K. Rode, Applied Physics Letters **111**, 102403 (2017), https://doi.org/10.1063/1.5001172.

[9] K. Borisov, D. Betto, Y.-C. Lau, C. Fowley, A. Titova, N. Thiyagarajah, G. Atcheson, J. Lindner, A. M. Deac, J. M. D. Coey, P. Stamenov, and K. Rode, Appl. Phys. Lett. **108**, 192407 (2016), 10.1063/1.4948934.

[10] M. Žic, K. Rode, N. Thiyagarajah, Y.-C. Lau, D. Betto, J. M. D. Coey, S. Sanvito, K. J. O'Shea, C. A. Ferguson, D. A. MacLaren, and T. Archer, Phys. Rev. B **93**, 140202 (2016).

[11] K. Vahaplar, A. M. Kalashnikova, A. V. Kimel, S. Gerlach, D. Hinzke, U. Nowak, R. Chantrell, A. Tsukamoto, A. Itoh, A. Kirilyuk, and T. Rasing, Phys. Rev. B **85**, 104402 (2012).

[12] A. R. Khorsand, M. Savoini, A. Kirilyuk, A. V. Kimel, A. Tsukamoto, A. Itoh, and T. Rasing, Phys. Rev. Lett. **110**, 107205 (2013).

[13] Y. Tsema, M. Savoini, A. Tsukamoto, A. V. Kimel, A. Kir-

ilyuk, and T. Rasing, Applied Physics Letters **109**, 172403 (2016), https://doi.org/10.1063/1.4966183.
[14] J. Kerr, Phil. Mag., Series 5 **3**, 321 (1877).
[15] D. E. Aspnes and A. A. Studna, Phys. Rev. Lett. **54**, 1956 (1985).
[16] K. Fleischer, R. Verre, O. Mauit, R. Sofin, L. Farrell, C. Byrne, C. Smith, J. McGilp, and I. Shvets, Phys. Rev. B **89**, 195118 (2014).
[17] T. Herrmann, K. Lüdge, W. Richter, K. G. Georgarakis, P. Poulopoulos, R. Nünthel, J. Lindner, M. Wahl, and N. Esser, Phys. Rev. B **73**, 134408 (2006).
[18] J. P. Cunniffe, D. E. McNally, M. Liberati, E. Arenholz, C. McGuinness, and J. F. McGilp, phys. stat. sol. (b) **247**, 2108 (2010).
[19] Y. V. Kudryavtsev, Y. Lee, and J. Rhee, Phys. Rev. B **66**, 115114 (2002).
[20] S. Halilov and E. Kulatov, J. Phys.: Condens. Matter **3**, 6363 (1991).
[21] J. Zak, E. Moog, C. Liu, and S. Bader, Phys. Rev. B **43**, 6423 (1991).
[22] H. Kurt, K. Rode, P. Stamenov, M. Venkatesan, Y.-C. Lau, E. Fonda, and J. Coey, Phys. Rev. Lett. **112**, 027201 (2014).
[23] R. M. Osgood, B. M. Clemens, and R. L. White, Phys. Rev. B **55**, 8990 (1997).
[24] A. Tillmanns, S. Oertker, B. Beschoten, G. Güntherodt, C. Leighton, I. K. Schuller, and J. Nogués, Appl. Phys. Lett. **89**, 202512 (2006).
[25] P. Johnson and R. Christy, Phys. Rev. B **9**, 5056 (1974).
[26] P. Y. Yu and M. Cardona, *Fundamentals of semiconductors* (Springer, 2005).
[27] D. Hobbs, J. Hafner, and D. Spišák, Phys. Rev. B **68**, 014407 (2003).
[28] O. Hunderi and R. Ryberg, J. Phys. F **4**, 2084 (1974).
[29] K. Fleischer, Phys. Rev. B. (2018), see Supplemental Material at URL for more details on the influence of Ru doping $x$ on the optical properties.
[30] J. Matsuno, N. Ogawa, K. Yasuda, F. Kagawa, W. Koshibae, N. Nagaosa, Y. Tokura, and M. Kawasaki, Science Advances **2** (2016), 10.1126/sciadv.1600304, http://advances.sciencemag.org/content/2/7/e1600304.full.pdf.
[31] K. Siewierska, N. Teichert, R. Schaefer, and J. Coey, IEEE Transactions on Magnetics (2018), in press.
[32] N. Awari, S. Kovalev, C. Fowley, K. Rode, R. A. Gallardo, Y.-C. Lau, D. Betto, N. Thiyagarajah, B. Green, O. Yildirim, J. Lindner, J. Fassbender, J. M. D. Coey, A. M. Deac, and M. Gensch, Applied Physics Letters **109**, 032403 (2016), https://doi.org/10.1063/1.4958855.

# Supplementary Information:

# Magnetooptical Kerr effect in a zero-moment ferrimagnet: The case of $Mn_2Ru_xGa$

K. Fleischer,[1,2] N. Thiyagarajah,[1,3] Y.-C. Lau,[1,3] D. Betto,[1,3] K. Borisov,[1,3]
C. M. Smith,[1] I. V. Shvets,[1,3] J.M.D. Coey,[1,3] and K. Rode[1,3]

[1] *School of Physics, Trinity College Dublin, Dublin 2, Ireland*
[2] *School of Physical Sciences, Dublin City University, Dublin 9, Ireland*
[3] *CRANN and AMBER, Trinity College Dublin, Dublin 2, Ireland*

## S1. Optical Modeling

As discussed in the manuscript the procedure to extract the individual components ($\tilde{\varepsilon}_{ij}$) of the complex dielectric tensor requires least square fitting of modelled $\tan\Psi$, $\cos\Delta$, $\theta_k$ values over the entire measured spectral range. The standard method to do this for multilayered samples are so called transfer matrix calculations. In ellipsometric measurements of thin films these are typically used to not only derive the dielectric function of a thin film, but can also be used to fit film thickness, surface roughness and other parameter.[1]

The spectral shape of each tensor component is typically described by a set of standard functions, with Drude oscillators, harmonic oscillators (Drude-Lorentz), Tauc-Lorentz or expressions for 1D, 2D, or 3D bulk critical points.[1,2] As the modelling describes the spectral shape of the dielectric functions over the whole spectral range there are often several ways to describe it. Here we have chosen the simplest form, with the least amount of free parameter, in order to investigate systematic changes with Ruthenium concentration. In addition we did not fit on any geometric parameter (film thickness, interface roughness) as these have been independently measured by X-ray reflectance. All other materials (Air, $AlO_x$, MgO) were described by tabulated bulk values of their respective dielectric function. To minimise the number of free parameters all films $Mn_2Ru_xGa$ films have been treated as optical isotropic ($\tilde{\varepsilon}_{xx}$=$\tilde{\varepsilon}_{yy}$=$\tilde{\varepsilon}_{zz}$).

In all cases fits began with refining spectra using a single Drude oscillator (two parameters: amplitude $A$ (proportional to plasma frequency) and broadening $\Gamma$ (inverse of scattering rate)). In a second step additional harmonic oscillators (Drude-Lorentz oscillator, three parameter each: amplitude $A$, broadening $\Gamma$, and position $\omega_0$) were added and subsequently refined until any addition of another oscillator did not change the $\chi^2$ value further. This way we ensure that the spectral shape is only described with the minimum number of free fitting parameter. As discussed in the main article for the description of the diagonal component of the dielectric function three such oscillators were required, one in the visible, one in the UV and one in the deep UV range.

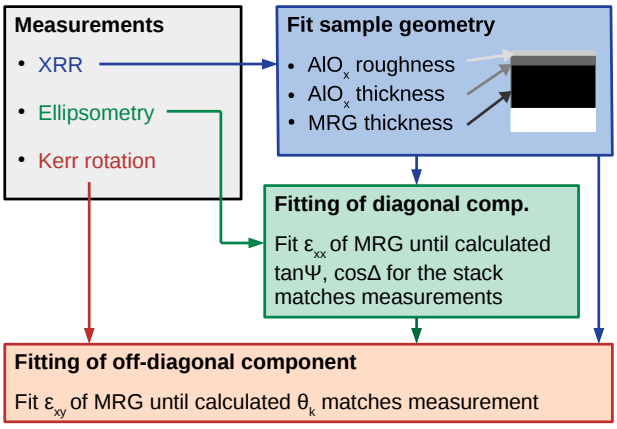


**Supplementary Figure S1.**
Schematic of the information flow for the optical modeling used to derive the tensor components for the dielectric tensor of $Mn_2Ru_xGa$. The procedure is done for each sample, to compare $\tilde{\varepsilon}_{xx}$, and $\tilde{\varepsilon}_{xy}$ as function of Ruthenium content.

Once the diagonal component was refined by the fits to the ellipsometric data for three angles of incidence, the off-diagonal component $\tilde{\varepsilon}_{xy}$ was fitted by calculating the complex Fresnel reflectance $r_x$ of an air/$AlO_x$/$Mn_2Ru_xGa$/MgO stack of known geometry using the refined $\tilde{\varepsilon}_{xx}$, and $r_y$ using $\tilde{\varepsilon}_{xx}$+$\tilde{\varepsilon}_{xy}$. $\theta_k$ is then simply derived from $\theta_k = Re(r_x - r_y)/(r_x + r_y)$. This equation is valid as we only analyse polar Moke of an optically isotropic medium, measured at near normal incidence. No dependece of the optical spectra on z-components of the dielectric tensor occur, nor difference between $\tilde{\varepsilon}_{xx}$ and $\tilde{\varepsilon}_{yy}$ are expected.[1,3] $\tilde{\varepsilon}_{xy}$ was likewise, initially described by a single Drude oscillator. Additional harmonic oscillators were added to minimise $\chi^2$. As for $\tilde{\varepsilon}_{xx}$ three oscillators were required to describe the spectral shape of $\tilde{\varepsilon}_{xy}$ and accurately describe $\theta_k$. However for $\tilde{\varepsilon}_{xy}$ two individual oscillators in the near infra-red and visible range, yet no DUV contribution were required.

All functions used to describe $\tilde{\varepsilon}_{xx}$ as well as $\tilde{\varepsilon}_{xy}$ are Kramers-Kronig consistent, hence represent meaningful physical fits of the underlying absorption processes, rather than simply reproducing the shape of the spectra. The procedure outlined here, implicitly treats any features in the spectral response of $\theta_k$ caused by variations in stack reflectance caused by the spectral shape of the dielectric function of all materials involved, as well as thickness related thin film interference structures.

## S2. Deconvolution of contributions to the dielectric tensor – dependence on Ru concentration

### 1. *Diagonal component $\varepsilon_{xx}, \sigma_{xx}$*

In the main article (Fig. 4) we show the dielectric function $\tilde{\varepsilon}_{xx}$ for several samples as extracted from least square fits of the measured $\tan\Psi$ and $\cos\Delta$. The deconvolution into several components, as shown in the article (Fig. 5)

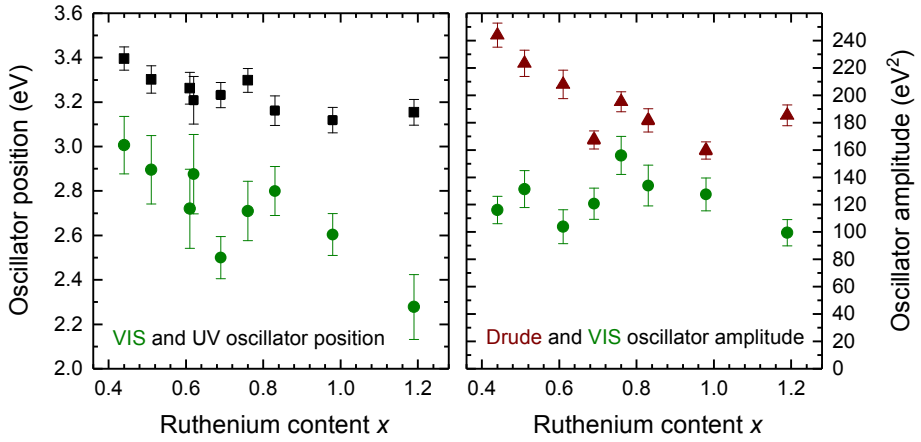


**Supplementary Figure S2.**
Dependence of selected parameter of the model dielectric tensor as function of the Ru content. Here we show parameter with a significant change upon increase of Ru content such as the energetic positions for the VIS and UV oscillator and the amplitude of the Drude and VIS oscillators.

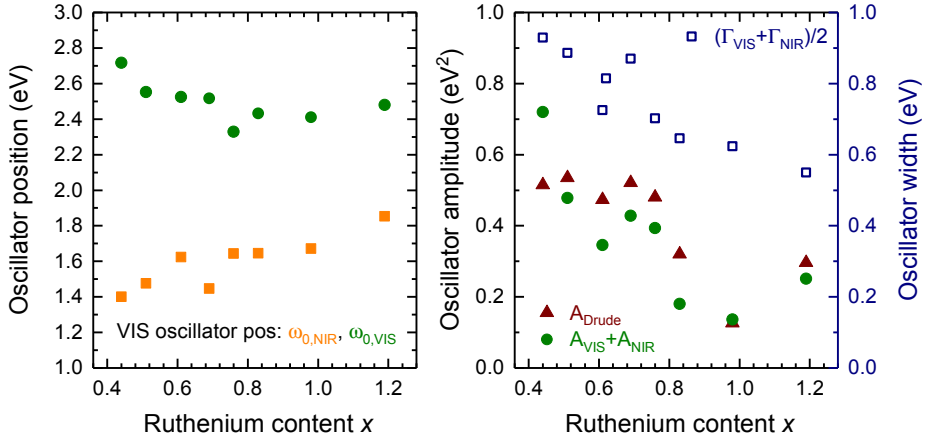


**Supplementary Figure S3.**
Spectral position of the two interband components used to describe $\tilde{\varepsilon}_{xy}$. Amplitude of the fitted interband and intra-band (Drude) components of $\tilde{\varepsilon}_{xy}$, as well as their average oscillator width ($\Gamma$). The energetic positions and line widths, again consistently change with the Ru content.

for a sample with $x = 0.61$, was likewise done for all investigated samples. We can therefore analyse the dependence of individual components on the Ru content.

Figure S1 shows selected parameters extracted from the dielectric model as function of Ru content. Both the Drude part as well as the main, VIS Oscillator are very broad, with a broadening parameter of the harmonic oscillator ($\Gamma \approx 5$-7 eV) larger than the measured range. As discussed, this is due to each model oscillator being a superposition of a larger number of unresolved optical transitions. An increase in Ru concentration leads to an apparent red shift of absorption structures, in particular for the VIS component, which we assign to Mn states. We have shown[4] that on increasing $x$, the bands originating from Mn in the 4*c* position (higher-energy final states) is preferentially filled by the added electrons. Consequently this reduces the number of unoccupied states, skewing the relative weights of the different oscillators contributing to the broad VIS absorption, leading to the red-shift in energy. The Drude component is also affected by the Ru content. The DC conductivity of $Mn_2Ru_xGa$ varies by approximately 30 %[5] when $x$ is changed from 0.6 to 1.0, consistent with our observation of altered amplitudes in the Drude tail.

The presence of two dominant interband absorption structures, as well as the amplitude of the inter-band transitions is very similar to previous reports on cubic $Ni_2MnGa$.[6] Noticeably the two distinct absorption structures are less well separated and much broader in $Mn_2Ru_xGa$ than for $Ni_2MnGa$, again due to Mn occupying two different crystallographic positions.

Broadening of optical transitions is generally associated with disorder and has been seen for $Ni_2MnGa$[6], as well as $Co_2CrAl$.[7] In our case the observed differences with increasing Ru content, are significantly smaller than those reported for e.g. amorphous to crystalline samples of $Co_2CrAl$.[7] In addition the peak widths of inter-band transitions are slightly decreasing with inclusion of Ru, consistent with a better atomic order, once the initially vacant 4d-sites are occupied. Crystalline long-range quality, determined by XRD, is similar for all samples, and we conclude that the variations with $x$ are dominated by changes of the local order and Mn band filling, rather than disorder.

### 2. *Off-diagonal component* $\varepsilon_{xy}, \sigma_{xy}$

Similarly the Kerr spectra show features in the IR, associated to the intra-band transitions (Drude-like tail). In contrast to $\tilde{\varepsilon}_{xx}$ the magnetic components $\tilde{\varepsilon}_{xy}$ are dominated by the two inequivalent Mn sites and more fine structure is resolvable. We therefore need two individual components to describe the broad VIS oscillator in the Kerr-spectra. These are assigned two involve the Mn-4*a* and Mn-4*c* respectively. Our previous XAS/MCD measurements[4] showed that the magnetic moment in $Mn_2Ru_xGa$ is entirely carried by Mn. To compare the spectral dependence of the off-diagonal component of the dielectric tensor

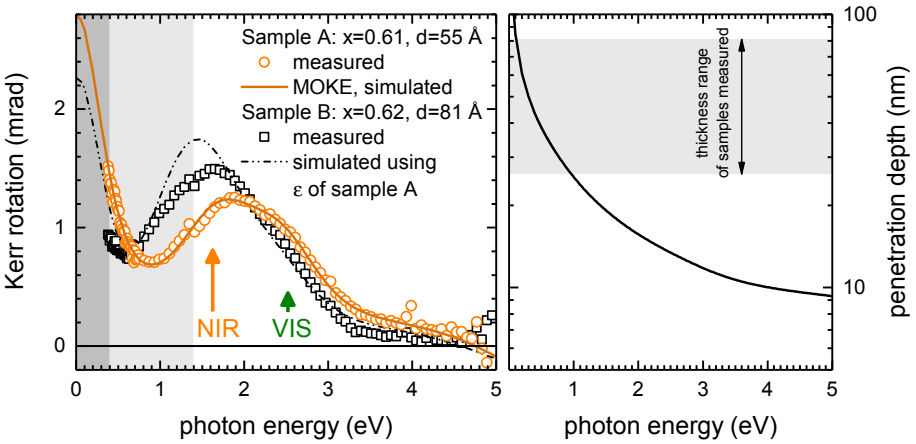


**Supplementary Figure S4.** Measured MOKE spectra of two samples with comparable $x$ but grown at different growth rates. The optical model of the thinner sample is used to calculate the expected MOKE of the thicker, highlighting the thickness dependence of the raw MOKE signal and the real change in magnetic order between the two samples. The right panel shows the penetration depth of light in $Mn_2Ru_xGa$ calculated from $\tilde{\varepsilon}_{xx}$ of a sample with $x = 0.61$. Please note the logarithmic scale.

$\tilde{\varepsilon}_{xy} = \pm iQm_z\tilde{\varepsilon}_{xx}$ between samples we only consider the magnitude of the Kerr rotation and only analyse fully saturated samples. After modelling the $\theta_k$ spectra using individual components in $\tilde{\varepsilon}_{xy}$, it is noticeable that all parameters show monotonic changes with $x$ (see Fig. S3). Particular the two features associated with interband transitions in the NIR-VIS (Mn) region show shifts in energetic position and amplitude, with distinctly different rate of change before and after $x \approx 0.7$. The latter has also been observed in the change of Mn 4$c$ magnetisation as function of $x$,[4] again suggesting that these particular optical transitions involve electronic states localised at the Mn sites. Likewise the fitted broadening of the structures is reduced with increasing Ru content as the number of crystal vacancies is reduced when $x$ approaches 1, and the local order is increased.

### S3. Thickness dependence in MOKE

For thin films there is no simple analytical equation to correlate the Kerr rotation $\theta_k$ to $\tilde{\varepsilon}_{xy}$. The film thickness for layers analysed here, varies between 26 and 81 nm. This coverage regime can not be treated either as thin film, nor optical thick layer as the layer thickness is not significantly larger than the penetration depth of light (see Fig. S4). Hence full optical transfer matrix calculations are required to fit the spectral form of $\tilde{\varepsilon}_{xy}$ to the measured $\theta_k$ spectra.[8] The main article Fig. 4 shows the raw MOKE measurements and Fig. 5 and 6 the model off-diagonal tensor components of the dielectric function (as fitted MOKE and in terms of $\sigma$).

The full optical modeling of the dielectric tensor components can now also be used to illustrate the dependency of measured $\theta_k$ spectra on the thickness of a thin film. Even with no changes in a materials electronic and magnetic properties, the spectral form and magnitude of the $\theta_k$ signal will strongly depend on the thickness of the thin film, as long as the light penetration depth is larger or in the same order as the film thickness. Figure S4 illustrates the expected Kerr rotation for varying film thickness. We show two nominally identical samples with different thickness, and then use the fit of the thinner sample to model the thicker. We find a very good agreement between the model and spectral features of the thicker sample, but difference in amplitude are observed. This illustrates the deviations in magnetic ordering between samples of different thickness as previously reported.[9] Independent from our discussion specific to $Mn_2Ru_xGa$ this illustrates the importance of employing optical models to quantitatively discuss sample properties in magnetic thin films, rather than discussing raw MOKE data.


[1] G. E. Jellison, in *Handbook of Ellipsometry*, edited by H. G. Tompkins and E. A. Irene (William Andrew Publishing, Norwich, NY, 2005) pp. 237 – 296.

[2] P. Y. Yu and M. Cardona, *Fundamentals of semiconductors* (Springer, 2005).

[3] T. Herrmann, K. Lüdge, W. Richter, K. G. Georgarakis, P. Poulopoulos, R. Nünthel, J. Lindner, M. Wahl, and N. Esser, Phys. Rev. B **73**, 134408 (2006).

[4] D. Betto, N. Thiyagarajah, Y.-C. Lau, C. Piamonteze, M.-A. Arrio, P. Stamenov, J. Coey, and K. Rode, Phys. Rev. B **91**, 094410 (2015).

[5] N. Thiyagarajah, Y.-C. Lau, D. Betto, K. Borisov, J. Coey, P. Stamenov, and K. Rode, Appl. Phys. Lett. **106**, 122402 (2015).

[6] Y. V. Kudryavtsev, Y. Lee, and J. Rhee, Phys. Rev. B **66**, 115114 (2002).

[7] Y. Kudryavtsev, V. Uvarov, V. Oksenenko, Y. Lee, J. Kim, Y. Hyun, K. Kim, J. Rhee, and J. Dubowik, Phys. Rev. B **77**, 195104 (2008).

[8] J. Zak, E. Moog, C. Liu, and S. Bader, Phys. Rev. B **43**, 6423 (1991).

[9] M. Žic, K. Rode, N. Thiyagarajah, Y.-C. Lau, D. Betto, J. M. D. Coey, S. Sanvito, K. J. O'Shea, C. A. Ferguson, D. A. MacLaren, and T. Archer, Phys. Rev. B **93**, 140202 (2016).